Thermal conductivity of disordered garnets from infrared spectroscopy

P. A. Giesting and A. M. Hofmeister
Department of Earth and Planetary Sciences, Washington University, St. Louis, Missouri 63130
(Received 25 July 2001; revised manuscript received 26 November 2001; published 4 April 2002)

The thermal conductivity (k) of garnets is calculated from a formula originating with Debye, adapted to treat the vibrations in a solid as a collection of damped harmonic oscillators. Our model utilizes phonon lifetimes obtained from Kramers-Kronig analyses of existing IR reflectivity spectra, as well as new data presented here, and calculates k at ambient conditions within a nominal uncertainty of 6% of the experimental values for eight natural samples with well-constrained chemical compositions. Agreement is good for the remaining garnets with uncertain compositions. Two series of natural mixed crystals were studied: (1) $X_3Al_2Si_3O_{12}$, where the X site has varying amounts of Mg, Fe^{2+}, and Ca and (2) $Ca_3Y_2Si_3O_{12}$, where the Y site has Al and/or Fe^{3+}. The model predicts k at ambient conditions for the end members. The occurrence of a minimum in k near the midpoint of each compositional series correlates with the maximum widths of the IR peaks. Thus, disorder on crystallographic sites largely controls the thermal conductivity of mixed crystals. We also tested the model using available data on synthetic yttrium garnets. Agreement is good for YAG. Observation of ~30% discrepancy between calculated and experimental k of YGG and YIG suggests that these unconfirmed measurements should be repeated.

DOI: 10.1103/PhysRevB.65.144305 PACS number(s): 66.70.+f, 78.30.−j

I. INTRODUCTION

Thermal conductivity (k) is an important material property. Geophysical applications require knowledge of k and its response to pressure, temperature, and phase[1] but progress is impeded because measurements of thermal conductivity are uncertain. Even at room temperature, differences of 20–30% occur in inter-laboratory comparisons.[2] Although theoretical approaches such as molecular dynamics explain certain attributes of thermal conductivity,[3] the accuracy is insufficient for most applications. We therefore have developed a semi-empirical model that relates thermal conductivity to spectroscopic data.[4,5] The present paper discusses the dependence of the lattice contribution at ambient conditions on chemical composition and site-substitutional disorder.

Debye[6] proposed that the thermal conductivity of an insulator could be obtained by equating phonon scattering to molecular collisions. This analogy to the kinetic theory of gases was developed by Peierls[7] and Klemens.[8] Most authors focused on the acoustic modes (see Ref. 5 for a review). The central shortcoming of these models is the lack of consensus regarding the phonon lifetimes, which were approximated in various ways from the Grüneisen parameter.[9] The calculations differ greatly from measurements at ambient conditions: discrepancies range from −70 to +430 % for simple rare gas solids and alkali halides (see tables in Ref. 10). Higher accuracy (−16 to +64 %) was obtained applying a different type of semi-empirical model, originating with Einstein,[11] to acoustic modes of glasses and various mixed crystals.[12] We did not pursue this approach because it assumes that no coherence exists between motions of neighboring atoms.

Optical modes were thought to be unimportant because their group velocity is zero at the center of the Brillouin zone (BZ). However, acoustic modes dissipate at temperatures above a few hundred kelvin through vibrational interactions,[13] optic modes have finite velocities inside the BZ,[14] and optic modes outnumber acoustic for all but the simplest structures, which means that optic phonons should not be neglected. Based on these observations, and on the association of low thermal conductivity with solids having a large number of optic modes, Hofmeister[4] used the damped harmonic oscillator model to obtain phonon lifetimes from widths of IR modes and to compute k. A simplified version of the formula for the lattice contribution at ambient conditions (k_0) reproduces measurements for phases with olivine and spinel structures.[5] The few experimental determinations that were not replicated are either obtained from poorly characterized samples or are inconsistent with other measurements.[15,16]

To test the revised formula against more complicated structures, and to examine the effect of site-substitutional disorder, the present paper applies the damped harmonic oscillator model to phases with the garnet structure. Garnets [general formula $X_3Y_2T_3O_{12}$] are important due to their technological and industrial applications,[17,18] ubiquitous occurrence in surface rocks,[19] and their likely existence deep inside the Earth.[20] The three cation sites (X, Y, and T) with their range of size and coordination numbers allow for an extensive variety of chemical substitutions. We benchmark the model against natural garnets because cooroborating thermal conductivity measurements exist.[9,16,17,21] We use existing IR reflectivity spectra[22–24] and provide new IR spectra for a thorough comparison. We predict k for samples lacking direct measurements, and evaluate k for synthetic garnets for which few confirmed measurements exist.

II. THE DAMPED HARMONIC OSCILLATOR MODEL FOR THERMAL CONDUCTIVITY

At room temperature only the lattice contribution to the thermal conductivity should be important. If heat is transferred randomly in local equilibrium, then the contribution of phonon scattering to thermal conductivity is obtained by analogy to the kinetic theory of gases.[6] Peierls[7] and

Klemens[8] derived summations of the form

$$k_{\mathrm{lat}}=\frac{1}{3}\frac{\rho}{ZM}\sum_{j=1}^{3}\sum_{i=1}^{3NZ}c_{ij}u_{ij}^{2}\tau_i, \tag{1}$$

where u_{ij} is the group velocity ($=\partial\omega_i/\partial q_j$, where $\vec{q}_j$ is the wave vector and $\omega_i=2\pi\nu_i$ is the angular frequency of a given mode), τ_i is the mean free lifetime between scattering events, ρ is the density, M is the molar formula weight, $i=1$ to $3NZ$ sums over the normal modes of a crystal with N atoms in the formula unit, Z formula units in the primitive cell, and $j=1$ to 3 represents the orthogonal directions. The Einstein heat capacity[25] of the ith vibrational mode,

$$c_{ij}=\frac{x_{ij}^{2}\exp(x_{ij})}{[1-\exp(x_{ij})]^{2}} \tag{2}$$

is calculated per mole and for constant volume; $x_{ij}=h\nu_i(\vec{q}_j)/k_BT$, h is Planck's constant, and k_B is Boltzmann's constant. IR and Raman modes are measured at $\vec{q}_j=0$, and the sum over j is assumed to be represented on average by these zone center parameters. The factor of $\frac{1}{3}$ in Eq. (1) is approximate, just as in the kinetic theory of gases.[26] The factor ρ/ZM provides the volume coresponding to that implicit in the summation. (The factor of Z was neglected by Hofmeister[4] as it does not affect the P and T derivatives.)

The following sections summarize how the components (c_i, u_i, and τ_i) are obtained. For details see Hofmeister.[5]

A. Lifetimes of optic modes

Phonon lifetimes can be extracted from IR reflectance spectra by modeling the vibrations as a sum of an appropriate number of damped harmonic oscillators,[27–29] each with frequency ω_i, damping coefficient Γ_i, and oscillator strength f_i. The complex dielectic function ($\epsilon=\epsilon_1+i\epsilon_2$) for n oscillators is

$$\epsilon_1=n_1^{2}+n_2^{2}=\epsilon_\infty+\sum_{j=1}^{n}\frac{f_j\omega_j^{2}(\omega_j^{2}-\omega^{2})}{(\omega_j^{2}-\omega^{2})^{2}+\Gamma_j^{2}\omega^{2}} \tag{3a}$$

and

$$\epsilon_2=2n_1n_2=\sum_{j=1}^{n}\frac{f_j\omega_j^{2}\Gamma_j\omega}{(\omega_j^{2}-\omega^{2})^{2}+\Gamma_j^{2}\omega^{2}}, \tag{3b}$$

where n_1 is the real part of the index of refraction, n_2 is the imaginary part, and $\Sigma f_j=1$. The transverse optic (TO_i) frequency ($\nu_i=\omega_i/2\pi$) occurs at maxima in $\epsilon_2(\nu)$ and the longitudinal optic (LO_i) frequency is determined from minima in the imaginary part of $1/[\epsilon_1(\nu)+i\epsilon_2(\nu)]$. The damping coefficient Γ_i is related to the lifetime

$$\frac{1}{\tau_i}=\Gamma_i=2\pi\times\mathrm{FWHM}, \tag{4}$$

where FWHM is the full width at half maximum, in frequency ν units, of each peak in $\epsilon_2(\nu)$. In this three-parameter description of the peaks, the LO_i frequency is a function of ν_i, Γ_i, and f_i. The oscillator strength is

$$f_i=\frac{\Gamma_i\sigma_i(\max)}{\pi\nu_i^{2}}, \tag{5}$$

where the conductivity is defined[27–29] as

$$\sigma(\nu)=\nu\epsilon_2(\nu)/2. \tag{6}$$

The above Lorentz model represents IR data extremely well,[30] even for complex substances with over 100 peaks.[31] Electron band systems are also amenable to the analysis.[14] The Lorentz model is widely applicable because the corresponding quantum mechanical equation for ϵ has the same form as the classical equation.[30,14]

Sometimes the fit requires other peaks in addition to the fundamental modes expected from symmetry.[30,32,33] The extra bands, arising through resonaces and overtone/combination modes, complicate classical dispersion analysis. Hence, a Kramers-Kronig analysis was used to extract the dielectric and optical functions.[27,28,34] Virtually the same values for Γ_i are obtained from Kramers-Kronig and classical dispersion analyses of reflectance for crystals[32] and glasses.[34] The robust nature of this method of analyzing IR reflectivity data is covered elsewhere.[35,36] For well-resolved peaks, the uncertainty in FWHM is similar to that of the TO frequency. Overlapping peaks present problems, but in these cases, the HWHM can be obtained.[23,33]

For the Raman modes, which have Lorentzian shapes, Eq. (4) should hold.[14] However, Raman line shapes are subject to instrumental broadening. IR data sufficed for determining the lifetimes for optic modes for olivine and spinels,[5] suggesting that IR spectra of garnets adequately represent all the optic modes.

B. Lifetimes of acoustic modes

Crystalline solids have three acoustic modes which can be probed through Brillouin spectroscopy. In theory, their lifetimes are also represented by Eq. (4). However, these linewidths are broadened by instrumental factors.[37] Brillouin spectra are collected where $\vec{q}$ is small.[38] At zone center, acoustic frequencies are zero, and their lifetimes (inverse with width) are infinite or undefined. The modes travel far, but have no energy, and thus this representation is not appropriate for calculation of k. Instead, zone edge values of FWHM are used to calculate k (as in calculations of C_V). Zone center values are appropriate for optic modes, but zone edge values are used for acoustic modes (for both k and C_V) because the acoustic modes are converted to optic modes through zone folding (i.e., doubling of the unit cell), and it is their zone edge value that is transferred to the zone center.[14]

The appearance of acoustic modes in IR spectra allows determination of their lifetimes directly from the dielectric functions. FWHM of the resonating acoustic modes are close to that of the IR modes.[32,33] Furthermore, the ratio FWHM/ν of 4.3 to 6.2% for olivine and spinel-type minerals obtained from Brillouin scattering is comparable to FWHM/ν of 2 to

4% determined for γ-Fe_2SiO_4 from IR data.[5,33] This ratio from IR data is smaller because IR widths are not affected by instrumental broadening. In lieu of direct measurement of acoustic modes, acoustic lifetimes can be estimated from the narrow widths of the weakest IR peaks.

C. Heat capacities of phonons

Equation (2) assumes that the atoms of the solid vibrate independently and at a constant frequency. Use of a constant frequency means that the group velocity is zero, and thus as regards Einstein heat capacities, the summation in Eq. (1) is made only over the number of modes. Summing c_i to obtain C_V provides the correct high-temperature limit, but the response at low temperature is more rapid than the experimentally observed T^3 dependence. Yet the agreement of Σc_i with C_V is reasonable,[14,39] even for the complex structures found in minerals.[40]

Debye[41] treated the crystal as an isotropic, continuous medium. The basis of the model is a linear relationship between angular frequency ω and wave vector $\vec{q}$. The extrapolation of the linear relationship to the zone edge provides the frequency used to compute C_V. Debye's model is an improvement over Einstein's, in that it reproduces the essential features of C_V, but it is not exact either.

More accurate formulations for C_V exist.[42,43] For the present model of thermal conductivity, little benefit is gained by using the more complicated equations. Einstein's formula suffices for optic and acoustic modes, and the effect of $\vec{q}$ on c_i can be neglected. Although Eq. (2) assumes noninteracting phonons, it should be valid when scattering is present. This claim is based on the quantum mechanical derivation of the Lorentz-Drude model, in which the frequency represents the transitions between states.[29] The frequency has the same meaning in interacting and noninteracting systems.

D. Speeds, frequencies, and participation of acoustic modes

For small $\vec{q}$, a linear relationship exists with ω: hence, the group velocity $\partial\omega/\partial\vec{q}$ equals the phase velocity ω/q.[38] Thus, near zone center, the longitudinal acoustic (LA) group velocity equals the speed u_P of the compression wave and the transverse acoustic (TA) group velocity gives the shear speed u_S. Acoustic frequencies at zone edge can be obtained either from extrapolation of Brillouin frequencies, or from using ultrasonic measurements of the sound speeds in Debye's formula [$\omega_{\mathrm{LA}}=u_P(6\pi^2NZ/V_{\mathrm{PC}})^{1/3}$ where V_{PC} is the volume of the primitive unit cell].

A reasonable representation of C_V is obtained by assuming that linear dispersion of the acoustic modes at zone center represents the entire Brillouin zone.[41] In calculating the closely related transport property k, linear dispersion is also a valid assumption, and the sound speeds (and corresponding frequencies near $\vec{q}=0$) are taken to represent the acoustic modes over the entire BZ. Given the approximations underlying Eq. (1), the directional dependence of u_i for the acoustic modes is an unneccessary complication.

Near the edge of the Brillouin zone, the frequency is constant and hence acoustic group velocities decrease from the sounds speeds at zone center to zero at the maximum values of $\vec{q}$. Potentially, the acoustic contribution to k could be overestimated from using linear dispersion in Eq. (1) by $\sim$25%. If a more realistic form for dispersion of the acoustic modes truly were needed, greater disparities would exist between Debye's and Einstein's C_V models, which utilize contrasting dispersion relations, and poorer agreement with experiment would exist. Neither effect is observed.[14,33,40] Overestimation of group velocities seems to be compensated for by other factors.

The role played by the acoustic modes is limited by the particular mechanism involved in heat exchange. Beyer and Letcher[13] (pp. 255–260) describe how compressional waves above about 100 K are attenuated through collisions with other phonons in the solid (thermoelastic loss) whereas TA phonons do not suffer thermoelastic losses because shear waves do not produce volume changes. Thus TA modes do not participate above $\sim$100 K. The LA phonons lose energy because heat is transmitted from the compressed (hot) to the rarefracted (cool) regions of the sample. (Different loss mechanisms pertain at cryogenic temperatures.) The importance of the acoustic modes in calculating k_0 for complex structures is further diminished by their scant number compared to the optic modes (237 for garnet).

E. Group velocities of the optic modes

In principle, the dependence of frequency on $\vec{q}$ for the various optic modes, determined through inelastic neutron scattering (INS) measurements or through theoretical models, could provide the information needed for the full summation in Eq. (1). However, the dispersion relations derived from INS trace only the peak centers of the LO and TO modes across the BZ. This description of phonon properties represents only the quasiharmonic aspects, i.e., the effect of phonon interactions is not revealed. Vibrational energy at $\vec{q}=0$ is not limited to isolated frequencies but is distributed between the LO and TO modes, and below to $\nu_{\mathrm{TO}}-\Gamma/2\pi$.[29] The finite peak width measured at zone center, which is related to phonon damping via collisions must also carry over to INS relations. Below is a qualitative analysis of the effect of interactions on group velocities.

From INS curves, the group velocities of optic modes are commonly smaller than those of acoustic modes, but are within a factor of 10 (e.g., Ref. 44). Similar group velocites are expected because no simple distinction exists between the optic and acoustic branches away from the critical points (zone center and edges),[14] and because optic branches are related to acoustic branches through folding of the BZ, which occurs, for example, when the unit cells are doubled by ordering.

Suppose that the dispersion of the optic modes is represented by their behavior near zone center. From the classical damped harmonic oscillator model, the mean value of u cannot be zero because the finite lifetime of the phonon suggests a finite group velocity. (Exactly at $\vec{q}=0$, a standing wave exists, but not at small $\vec{q}$: excitation of phonons by photons

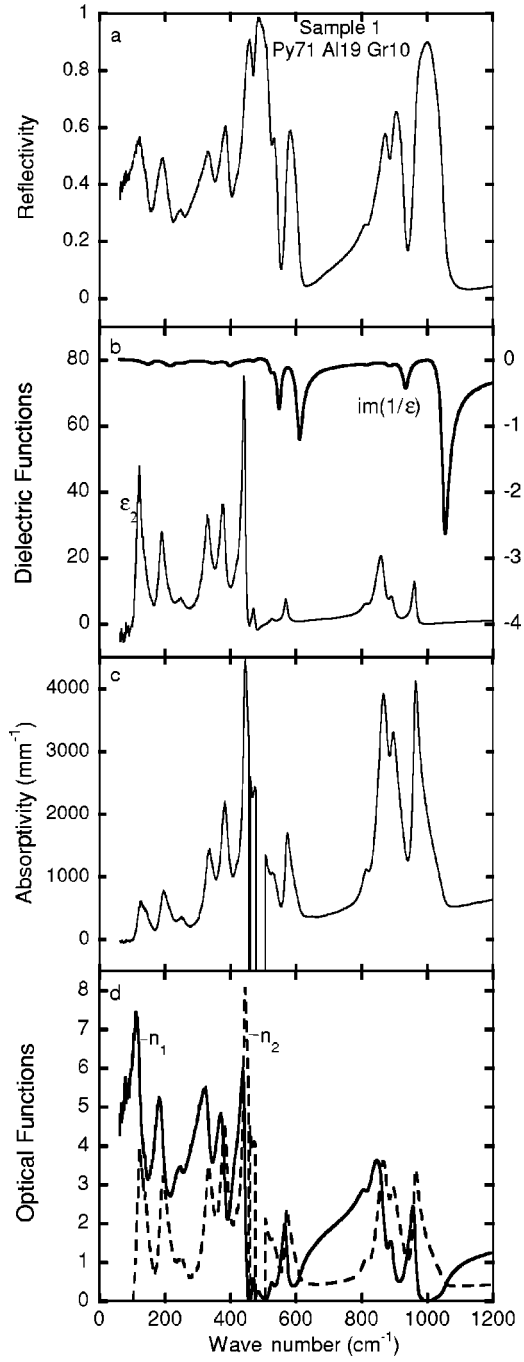

FIG. 1. IR spectra and derived functions for sample 1 (see Table II). Sample composition at top of figure. (a) Raw reflection data. (b) Calculated values of dielectric functions ϵ_2 (thin line) and im$(1/\epsilon)$ (thick line; values along right axis). (c) Calculated absorbtivity values. (d) Calculated values of the real and imaginary parts of the index of refraction $(n_1+in_2;\ n_1$ is the solid line, n_2 is the dashed line). The calculated data reveals problems with the analysis around 450–500 cm^{-1} due to poorly resolved peaks.

requires small $\vec{q}$ for an interaction.) For frequency regions distant from the absorbing frequencies, the dielectric function is real where $\epsilon_2 = 0$ (Fig. 1). In these transparent regions above and below the TO frequency, the group velocity equals the phase velocity[14] $[u_i=\omega_i/q_i=c/n_1(\omega_i)]$. These high group velocities are a consequence of the dielectric constants varying spatially as well as depending on frequency.[14,29] Hence, over each IR peak, a value similar to the sound speed is one possible average of these two extremes 0 and c/n_1. The mean group velocity should be closer to 0 than to c/n_1 because $\epsilon_2=0$ at frequencies distant from the peak, whereas on the edges of the peak, ϵ_2 is small and the group velocity is reduced.

For each peak, the dispersion relationship is[14]

$$\vec{q}\cdot\vec{q}=\epsilon\left(\frac{\omega}{c}\right)^2. \tag{7}$$

Differentiating Eq. (7) gives

$$u=\frac{\partial\omega}{\partial q}=\frac{c}{\epsilon^{1/2}(1+(qc/2\epsilon^{1/2})\partial\epsilon/\partial\omega)}. \tag{8}$$

The dependence of ϵ on ω in the damped harmonic oscillator model is complicated [Eq. (3)], so as a first approximation, u goes as $c/\epsilon^{1/2}$ plus other terms. Substituting Eq. (7) into Eq. (8) yields

$$u\sim\omega/q\propto\nu a, \tag{9}$$

where a is a lattice constant. This approximate formula for group velocities of the optic modes as classical damped harmonic oscillators has the same functional dependence as Deybe's dispersion relationship for the acoustic modes. Equation (9) overestimates u (as $\sim$100 km/sec) because the denominator in Eq. (8) was neglected during differentiation.

Alternatively, one could argue that polaritrons are observed in IR reflectivity experiments, i.e., the phonons and photons are coupled.[14] For polaritrons at low q, the group velocity equals c/n_1 where n_1 is obtained for frequencies below ν_{TO} (i.e., the low-frequency limit is used for a solid with one vibration). The group velocity rapidly increases from 0 for $\vec{q}=0$ to these large values.[14] The average value over the zone again lies somewhere between these extremes.

Because INS curves provide group velocities that are appropriate for noninteracting phonons, and because only approximate values for u at small $\vec{q}$ can be inferred from the damped harmonic oscillator model, we assume that the optic modes are represented by an average speed $\langle u\rangle$. For phases with the olivine structure, which has 84 vibrational modes, or for spinels, which have 42 total modes, a simple average, $\langle u\rangle=(u_S+u_P)/2$, resulted in an accurate description of k.[5] For garnets, with a larger number of total modes (240), a weighted average, that accounts for double degeneracy for the shear wave, is proposed:

$$\langle u\rangle=\frac{2u_S+u_P}{3} \tag{10}$$

in anticipation of a larger number of interactions and slower group velocities.

TABLE I. Source data for samples with new spectral data presented in this paper.

Sample [a]	Approx. composition [b]	Source ID	Locality and notes
1	$Py_{71}Al_{19}Gr_3Uv_3An_4$	SFS4[c]	Frank Smith Kimberlite, South Africa [e]
10	$Py_{47}Al_{40}Gr_{13}$	SBB23[c]	Bobbejaan Kimberlite, South Africa
14	$Py_{52}Al_{20}Gr_{22}An_4Uv_2$	SRV4[c]	Roberts Victor Kinberlite, South Africa [f]
16	$Py_{41}Al_{45}Sp_1Gr_{13}$	SM 1348 [d]	Gore Mountain, Essex Co., NY [g]
2	$Gr_{99.5}Al_{0.5}$	[c]	Georgetown, CA [h]

[a]For details see Hofmeister *et al.* (Ref. 57).
[b]From data in Table 1a [EPAPS deposit (Ref. 60)].
[c]Provided by R. M. Hazen and J. R. Smyth.
[d]From the U. California, Davis, mineral collection.
[e]Also see Boyd (Ref. 75).
[f]Also see Capoiscio and Smyth (Ref. 76).
[g]Also see Levin (Ref. 77), Deer *et al.* (Ref. 19), p. 50.
[h]Also see Pabst (Ref. 78).

F. A simple formula for the thermal conductivity of insulators at ambient conditions

Because the optic group velocities may be represented by an average, and because the lifetimes of individual peaks[33] vary little (also shown below) Eq. (1) simplifies. The sum over the directions is ignored as only the bulk value of k is sought and the dependence on $\vec{q}$ is assumed to be represented by zone center behavior, giving

$$k_0=\frac{1}{3}\frac{\rho}{ZM}\langle u\rangle^2\tau\sum_{i=1}^{3NZ}c_i=\frac{1}{3}\frac{\rho}{ZM}\frac{\langle u\rangle^2}{\langle\Gamma\rangle}C_V. \qquad (11)$$

All parameters are at ambient conditions.

Considering the frequency dependence of the terms in Eq. (11) supports the validity of converting the sum to an average. From Eq. (9), u_i is proportional to frequency. From Eq. (2), c_i varies inversely, but weakly, with ν_i. An inverse relationship between τ_i and ν_i[12]provides a lower limit to τ_i as it is equivalent to critical damping.[45] Hence $u_i^2\tau_i c_i$ goes as $\nu_i^2/\nu_i/\nu_i=1$.

Using an average [Eq. (11)], as Debye[6] proposed, rather than a sum [Eq. (1)] is justified because average properties are used in the kinetic theory of gases. Peierls[7] and subsequent researchers used summations because the models concerned only the three acoustic modes. But for a large number of vibrational modes, averaging is preferable. For garnets, with 3 acoustic and 237 optic modes, the acoustic modes can be ignored, and the average FWHM of the IR modes is assumed to represent all optic modes.

III. STRUCTURE AND SYMMETRY ANALYSIS OF GARNET

The garnet structure is depicted by alternating corner-linked TO_4 tetrahedra and YO_6 octahedra, with the X cations housed in distorted dodecahedral interstices.[46] Edge sharing is present between the dodecahedral sites and the octahedral and tetrahedral sites.

Natural silicate ($X_3Y_2Si_3O_{12}$) garnets typically have divalent X cations and trivalent Y cations. Two distinct compositional series (pyrope $[Mg_3Al_2Si_3O_{12}]$-almandine $[Fe_3Al_2Si_3O_{12}]$ and grossular $[Ca_3Al_2Si_3O_{12}]$-andradite $[Ca_3Fe_2Si_3O_{12}]$) dominate.[46] The two series result from the mismatch in size between the Ca ion and the smaller Mg and Fe ions and from the manner in which the edge-sharing polyhedral distort to accommodate these substitutions,[47,48] but pyrope-almandines usually contain some Ca, whereas Mg and Fe^{2+} can occur in grossular-andradites. In some of our samples, subordinate amounts of spessartine $[Mn_3Al_2Si_3O_{12}]$ and uvarovite $[Ca_3Cr_2Si_3O_{12}]$ are also present. Also, in the Ca-rich garnets, H^+ ions commonly and extensively replace Si^{4+}, creating hydrogarnets.[49,50] For convenience, compositions (Table I) are simplified to mole % of the end members, e.g., $Py_{70}Al_{15}Sp_5Gr_5An_3Uv_2$.

In synthetic garnets, yttrium occupies the X sites, while another trivalent metal ion species (Al, Fe, or Ga) occupies both the Y and T sites. Electronic properties are altered by replacing yttrium by lanthanide ions.[18,51,52] Our YAG sample contains 5.5% Sm.

The garnet structure is isometric, space group $Ia\bar{3}d$. The species found at Brillouin zone center are $3A_{1g}(R)+5A_{2g}+8E_g(R)+14T_{1g}+14T_{2g}(R)+5A_{1u}+5A_{2u}+10E_u+17T_{1u}(IR)+16T_{2u}$, where R denotes Raman active bands, and IR denotes infrared active bands. An additional acoustic mode of T_{1u} symmetry is split into one longitudinal and two transverse components. From site-group analysis,[53,54] the IR modes are assigned to the following motions: $1\,\nu_2=$O-T-O symmetric tetrahedral bend; 3 $\nu_3=T$-O asymmetric tetrahedral stretch; 3 $\nu_4=$the O-T-O asymmetric tetrahedral bend; 2 $R=$rotation/libration of the TO_4 tetrahedra; $2T=$translation of T_4 tetrahedra; and $2T_X$ and $3T_Y=$translations of the dodecahedral and octrahedral cations. This approximation neglects mode mixing. Symmetry analysis cannot be used to predict activity of an overtone because the anharmonic interactions producing overtones and combinations are not restricted by selection.[30] Our band assignments present the simplest combinations and additions that describe the overtones.

Some of our samples are irregularly birefringent. Such optical anomalies have been taken as indicating symmetry reduction through partial ordering of cations on the X and/or Y sites,[55] but also have been interpreted as originating in strain.[56,57] The IR spectra of optically anomalous samples show no departure from cubic symmetry,[58] and some birefringent samples are metrically cubic,[59] and thus we obtained and analyzed IR spectra of the garnets assuming that they were cubic.

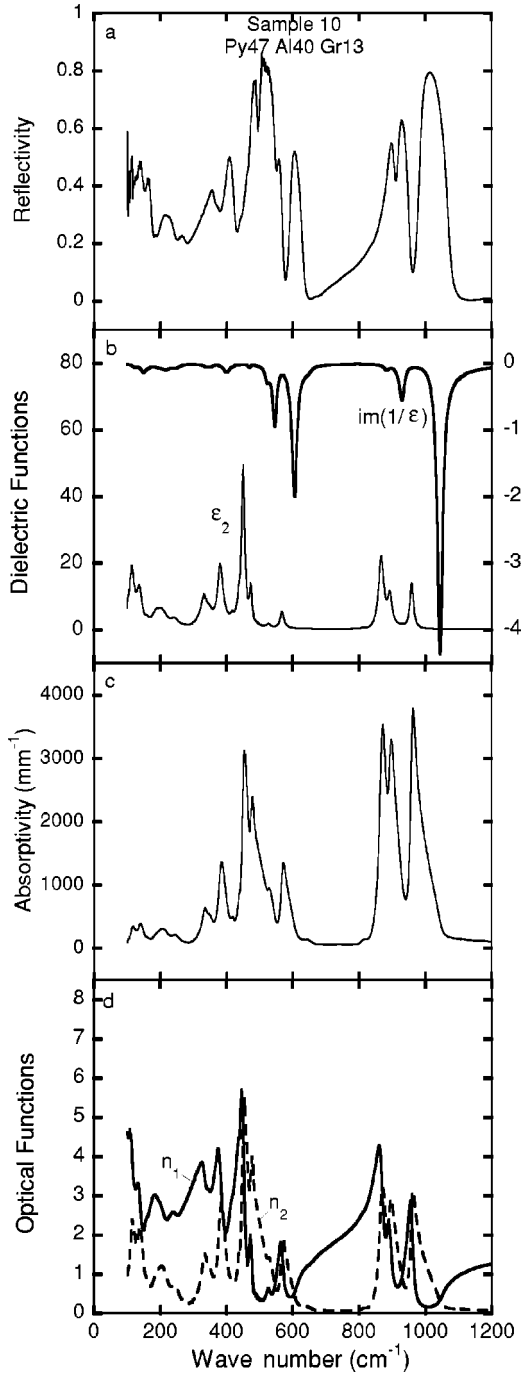

FIG. 2. IR spectra for sample 10. Functions presented as in Fig. 1.

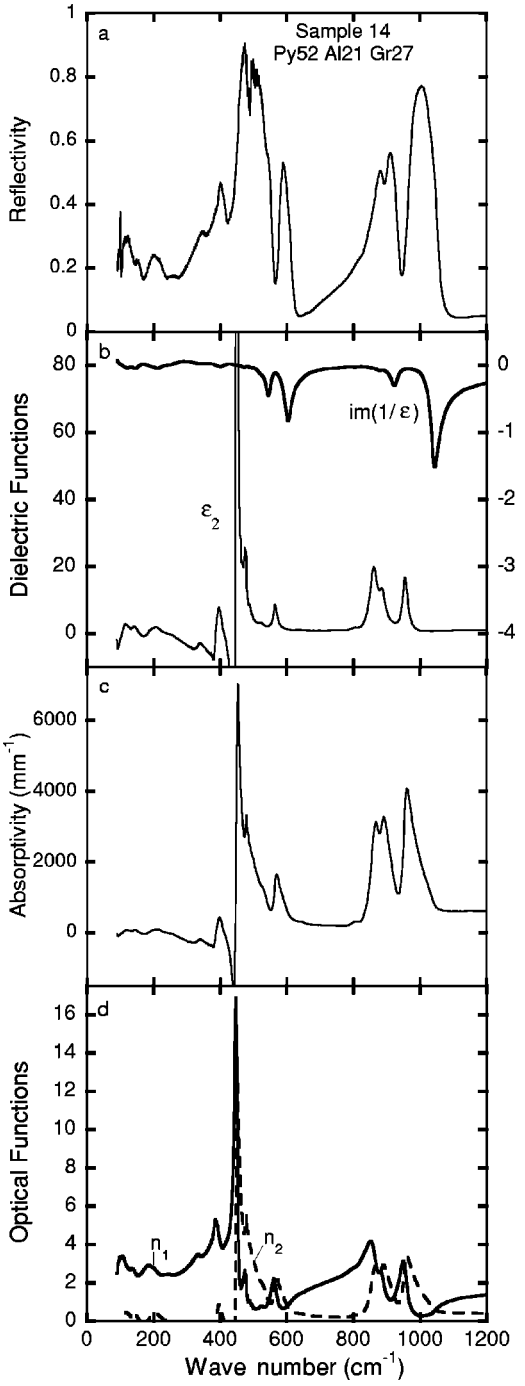

FIG. 3. IR spectra for sample 14. Functions presented as in Fig. 1. Strong overlapping peaks near 450 cm^{-1} make the analysis for lower wave numbers untrustworthy.

IV. EXPERIMENTAL PROCEDURE

New IR data were obtained from the samples described in Table I. Chemical analyses (Table 1a, accessible by EPAPS[60] or from the authors) were obtained with a Cameca SX-50 Electron Microprobe at the University of California-Davis using standard techniques.[23] Operating conditions consisted of a 15 KeV acceleration voltage, 10 nA current, and 10 second counting times. Chemical zonation was not observed.

Infrared reflectance spectra were obtained at ambient temperature using an evacuated Bomem DA3.02 Fourier transform interferometer (FTIR). We used an HgCdTe detector and a KBr beamsplitter for the range of 450–4000 cm^{-1} at a resolution of 1.0 cm^{-1}, or a silicon bolometer and mylar beamsplitters (3, 6, or 12 μm) for wavenumbers below 600 cm^{-1} at a resolution of 2.0 cm^{-1}. Between 1500 and 3000 scans were collected from each sample. Spectra were collected using a Spectratech FTIR microscope from samples of 1 to 12 mm diameter with random crystal orientation that were polished on one side. A Kramers-Kronig analysis[27,28] was performed on merged reflectance spectra using Wooten's approximation for extrapolating R to high frequency[29] and by

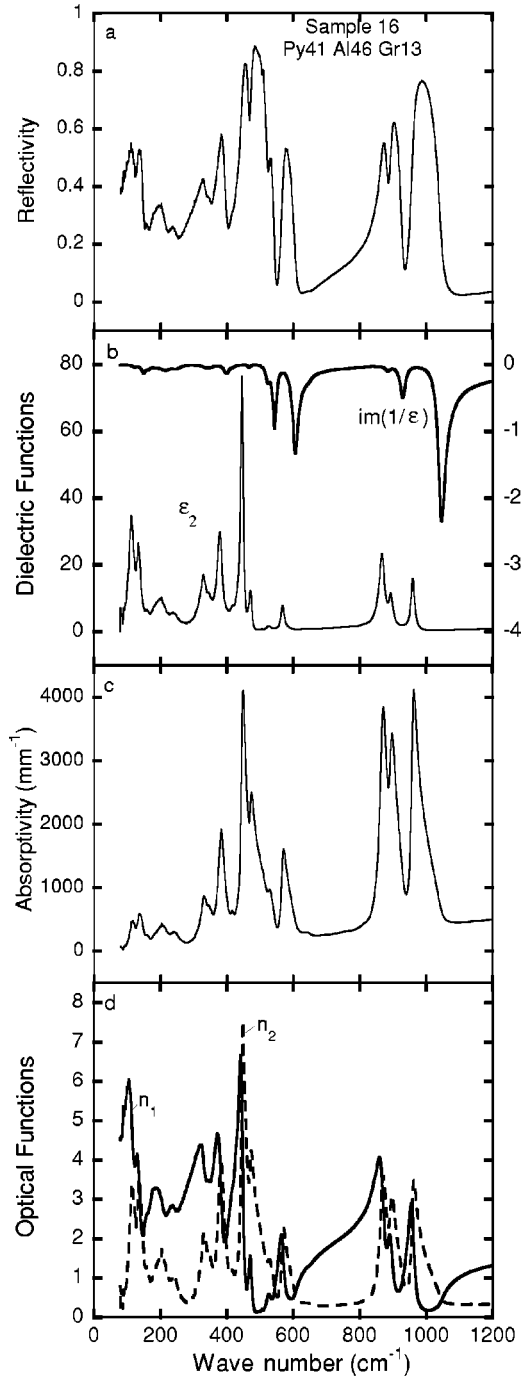

FIG. 4. IR spectra for sample 16. Functions presented as in Fig. 1.

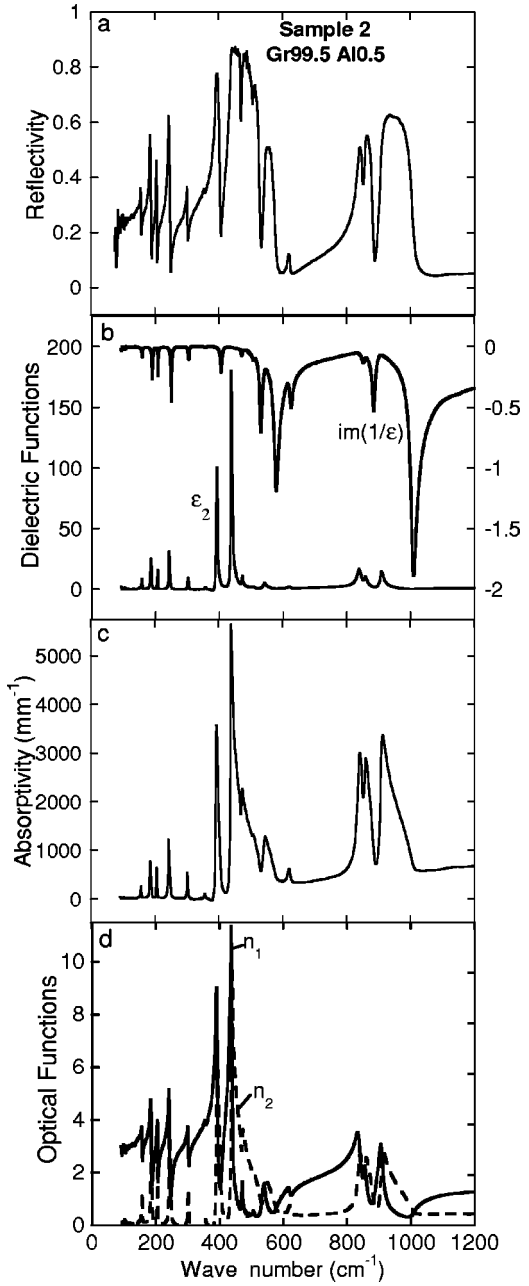

FIG. 5. IR spectra for sample 2. Functions presented as in Fig. 1.

assuming R is constant below the range of measurements. We also approximated R as being constant at high frequency for 6 of the samples, and found little to no change in the average peak width. Parameters are extracted as described in Sec. II. Uncertainties in peak positions are ± 0.1 to 1 cm^{-1}. Absorbancies were calculated using

$$\alpha(\nu) = \frac{2\pi\nu\epsilon_2(\nu)}{n_1(\nu)}. \tag{12}$$

Procedural details were given previously.[54]

V. SPECTROSCOPIC RESULTS

The IR spectra (Figs. 1–5) are consistent with previous studies of silicate garnets. Three strong peaks attributed to the Si-O stretch are observed in the 800–1000 cm^{-1} region, a cluster of strong peaks occur in the region of O-Si-O bending at $\sim$400–600 cm^{-1}, and many weaker peaks associated with the more loosely bound X cations are seen at lower wave numbers. The pattern of intensity in Figs. 1–4 resembles the pattern observed for pyrope-almandines,[23] although our samples have notably higher Ca content. Sample 14, with the highest grossular content, deviates the most from the general pattern. In the 400–500 cm^{-1} region, several strong peaks overlap, which is responsible for the

TABLE II. Spectral data for samples not previously published. Mode assignments are those for almandine in Hofmeister and Chopelas (Ref. 54) after Tarte (Ref. 61) and Moore *et al.* (Ref. 53). TO: transverse optic wave number. LO: longitudinal optic wave number. FWHM: full width at half maximum of transverse optic peak. *f*: oscillator strength from Eq. (4).

	1-$Py_{71}Al_{19}Gr_{10}$ [a]				10-$Py_{47}Al_{40}Gr_{13}$				16-$Py_{41}Al_{46}Gr_{13}$ [b]			
	TO	LO	FWHM	*f*	TO	LO	FWHM	*f*	TO	LO	FWHM	*f*
$B(\nu_3)$	960.6	1054.4	14.4	0.196	960.2	1045.7	12.8	0.187	959.4	1047.2	12.8	0.212
$C(\nu_3)$	891.1	885.6	19	0.180	893.4	885.0	16	0.210	892.9	886.1	14.6	0.190
$D(\nu_3)$	858.9	933.3	32	0.771	867.6	930.1	18.8	0.481	866.7	930.0	20	0.537
overtone	813.0				814							
overtone					774							
$E(\nu_4)$	~653				644.5	645.9	22.2	0.015	643	647	22	0.031
$F(\nu_4)$	569.2	611.5	12.2	0.164	567.9	606.2	13.3	0.130	568.3	607.5	11.7	0.162
$G(\nu_4)$	526.9	548.4	13	0.037	526.6	546.2	11.8	0.041	526.7	544.3	11	0.036
Ggr(ν_4)									506.9	506.9		
$H(T_Y)$	470.6	469.9	10	0.098	473.6	470.2	10	0.294	470.9	468.3	9.5	0.244
$I(\nu_2)$	441.1	525.0	13.3	2.26	450.7	524.3	12.6	0.376	445.5	524.4	9.4	1.61
overtone					432				432			
$J(T_Y)$	~420				419.2	420	6	0.083	416	416	9	0.170
$K(R)$	376.4	399.0	19	1.83	380.8	400.9	16.6	0.859	379.1	400.8	16.4	1.72
$L(R)$					347	349.7	8		346	349.2	11	0.372
$M(T)$	330.2	348.2	20.7	2.07	332.4	340.6	20.8	0.670	329.5	337.3	17.8	0.916
$O(T_Y)$	249.2	254	20	0.637	243	248.8	26	0.396	240	248.0	26	0.613
$N(T_X)$	191.4	217	21.1	3.07	200.1	217.6	34.1	0.615	203.8	216.3	24	1.20
$P_{Mg}(T_X)$					183.8	217.6	13.3	0.077	182	216.3	10	
$Q(T_X)$	140.2	148.4	9	1.30	136.9	150.0	16	1.58	159.1	162.7	9.4	0.405
$P_{Fe}(T_X)$		~163			158.4	162	12	0.348	132.3	148.8	17.2	3.43
$R(T)$	121.7	130	17.6	6.94	114.9	125.0	24	4.05	112.2	123.0	18	5.57

	14-$Py_{52}Al_{20}Gr_{22}An_4Uv_2$				2-$Gr_{99.5}Al_{0.5}$			
Mode	TO	LO	FWHM	*f*	TO	LO	FWHM	*f*
$B(\nu_3)$	955.5	1045	17.2	0.302	909.4	1009.0	13.7	0.191
$C(\nu_3)$	885.6	875	22.8	0.348	857.9	884.7	8.2	0.103
$D(\nu_3)$	861.8	923	26.4	0.606	838.3	885.0	12.1	0.149
$E(\nu_4)$	644	~648	18	0.0307	618.8	625.0	10.5	0.0187
$F(\nu_4)$	565.6	605.2	13.3	0.202	541.8	578.3	12.1	0.0875
$G(\nu_4)$	523	545.2	14	0.0867	506.6	506.7	9.4	0.0223
$H(T_Y)$	475.6	472	9	0.484	471.6	468.9	7.9	0.184
$I(\nu_2)$	449	521.7			437.2	530.0	4.7	1.94
$J_g(T_Y)$					432		~2	~0.08
$K(R)$	~376	~398			391.9	404.4	4.6	1.18
$L(R)$	~360				356.5	355.6	5.0	0.0250
$M(T)$	~335	~340			302.0	302.5	3.0	0.0931
$N(T_X)$					242.5	247.5	3.5	0.452
$O(T_Y)$	~240	~250			[c]	[c]	[c]	[c]
$P_{Ca}(T_X)$					206.0	207.8	2.0	0.154
$N(T_X)$	194							
$Q(T_X)$	~134	~144			185.0	189.4	3.0	0.409
$R(T)$	~100	~115			156.7	158.9	2.7	0.148

[a]The Gr component includes small amounts of An and Uv, see Hofmeister *et al.* (Ref. 57) for precise compositions.

[b]The Al component also includes Sp.

[c]*N* and *O* peaks assumed to be accidentally degenerate. Peak width is therefore counted twice in the average, which may slightly overestimate the average FWHM.

TABLE III. Experimentally derived values for the thermal conductivities of garnets, physical data for those garnets, and spectral widths from garnet samples of comparable composition. ρ: density; C_V: heat capacity; u_P and u_S: longitudinal and transverse sound speeds; expt. *k*: value for thermal conductivity listed in source or calculated from thermal diffusivity given in source; calc. *k*: model value for thermal conductivity calculated using the data in this table; No.: spectral sample number; W_{ave}: average full width at half maximum of ϵ_2 peaks (see Table II). If density is estimated, value was obtained from interpolation using values in Deer *et al.* (Ref. 19).

Sample	Composition [m]	ρ g/cm^3	C_V [n] J/mol K	u_P km/s	u_S km/s	expt. *k* W/m K	calc. *k* W/m K	No. [x]	W_{ave} cm^{-1}
SO SP [f]	$Py_{77}Al_2Sp_{21}$	3.72	330.0	8.92 [v]	5.55 [v]	4.30 [y]	3.94	18	12.9
H443 [a]	$Py_{70}Al_{20}Gr_{10}$	3.75	329.9	8.90 [u]	5.00 [u]	3.18	2.98	1	17.0
KG1 [b]	$Py_{56}Al_{38}Gr_6$ [h]	3.86 [h]	332.8	8.83 [s]	4.96 [s]	3.23 [w]	3.44	40	14.6
CBS [c]	$Py_{52}Al_{32}Gr_{16}$	3.82	332.2 [o]	8.82 [t]	4.98 [t]	2.90 [w]	3.01	10	16.5
Diment [d]	$Py_{53}Al_{47}$	3.93	334.1	8.77 [u]	4.94 [u]	2.03	3.03	10	16.5
SO AL [f]	$Py_{49}Al_{49}Sp_2$	3.95	334.6	8.77 [u]	4.94 [u]	4.30 [y]	3.31	33	15.1
SO RH [f]	$Py_{44}Al_{56}$	3.99	335.7	8.77 [u]	4.93 [u]	4.50 [y]	3.32	33	15.1
H123 [a]	$Py_{41}Al_{46}Gr_{13}$	3.93	334.5	8.77 [u]	4.93 [u]	3.31	3.30	16	15.0
KG2 [b]	$Py_{40}Al_{46}Gr_{14}$ [h]	3.92 [h]	334.5	8.77 [u]	4.93 [u]	3.14 [w]	3.29	16	15.0
Dreyer [e]	Al_{100}?	4.32	343.3	8.43 [v]	4.73 [v]	3.60	4.86	41	9.6
H20 [a]	$Gr_{30}An_{70}$	3.75	345.4	8.47 [u]	4.96 [u]	3.09	3.24	B44	13.5
H432 [a]	$Gr_{75}An_{23}Al_2$ [i]	3.32 [l]	335.5	9.04 [u]	5.30 [u]	5.19	4.01	B28	11.5
SO HS	$Gr_{90}An_3Al_7$ [k]	3.65	331.8	9.21 [v]	5.42 [v]	7.00 [y]	5.90	EDN	8.9
H700 [a]	$Gr_{91}An_9$ [j]	3.62	332.2	9.21 [v]	5.42 [v]	5.65	5.17	B51	10.1
H19 [a]	$Gr_{95}An_5$ [i]	3.55	331.3	9.26 [v]	5.46 [v]	5.62	5.98	B24	8.7
SO GR [f]	$Gr_{96}Al_3Sp_1$ [k]	3.62 [k]	330.7	9.27 [v]	5.46 [v]	7.20	7.16	B12	7.4
YAG [g]	$Y_{95}Yb_5AG$	4.64	371.2 [p]	8.52 [p]	4.97 [p]	7.85 [y]	8.85	YAG:Sm	5.3
YAG [f]	YAG	4.55	371.2 [p]	8.52 [p]	4.97 [p]	10.3	8.86	YAG:Sm	5.3
YIG [f]	YIG	5.29	426.4 [q]	7.41 [q]	4.30 [q]	7.40	3.97	YIG	9.7
YGG [f]	YGG	5.66	414.1 [r]	7.39 [r]	4.30 [r]	9.00	6.31	YGG	5.8

[a]Horai (Ref. 16).

[b]Kanamori *et al.* (Ref. 21).

[c]Chai *et al.* (Ref. 9).

[d]Diment and Pratt (Ref. 65); composition of sample estimated from density.

[e]Dreyer (Ref. 66). Sample described as ''almandine,'' no other data given. Physical parameters are for pure almandine. See discussion in text.

[f]Slack and Oliver (Ref. 17).

[g]Patel *et al.* (Ref. 18).

[h]Compositions and densities recalculated from their cell parameter and refractive index after Deer *et al.* (Ref. 19) Compositions given in source (Ref. 21) [KG1–$Py_{60}Al_{40}$; KG2–$Py_{50}Al_{50}$] are not consistent with their given physical data, whether considered together or singly. Grossular was assumed as the third phase for reasons explained in the text.

[i]Compositions from samples at the same localities in Rossman and Aines (Ref. 49).

[j]Composition estimated from density. Garnet from a similar locality was described by Agar and Krieger (Ref. 79) as $Gr_{84}An_{11}PAS_5$, where PAS is combined pyrope, almandine, and spessartine content.

[k]The composition listed in Slack and Chrenko (Ref. 69) explicitly ignored Fe^{3+} (An) content although they noted the characteristic bands in the samples' spectra. Inspection of those spectra led to the given estimates of An content; the compositions are otherwise as listed in the source. Density is estimated from these compositions.

[l]Low density presumably indicates inclusion of H_2O as hydrogarnet (Refs. 19, 49). If sample were grossular (no Fe^{3+}), density corresponds to 0.6 Si^{4+} per formula unit replaced by $4H^+$. Barring impurities, this is a minimum value for the H^+ content of this garnet; such samples are known, though not common, and the presence of impurities (nongarnet phases) in this sample is not unlikely. Molar weight is lowered to correspond to hydrogarnet content.

[m]Molar weights were calculated form the composition, see Table IV for examples.

[n]Interpolated from endmember values: pyrope (Ref. 54), almandine, grossular, and andradite (Ref. 80).

[o]Chai *et al.* (Ref. 9) calculated C_p=358.9 J/mol K. Given the endmember values used above, and assuming nearly ideal mixing (Ref. 63), this value is too large.

[p]Yogurtçu *et al.* (Ref. 81).

[q]Eastman (Ref. 82).

[r]Zharikov *et al.* (Ref. 83).

[s]For garnet with composition Py62 Al36 Gr2 (Ref. 73).

[t]Chai *et al.* (Ref. 74).

[u]See Babuška *et al.* (Ref. 67), for a garnet with a similar composition.

[v]Interpolation or extrapolation from existing data.

[w]Calculated using thermal diffusivity of source and calculated heat capacity listed in the table.

[x]Compositions in the other tables.

[y]Value for *k* inferred from the figure.

[z]Because Fe^{2+} (Al) and Mn^{2+} (Sp) are so similar, in the absence of any available IR data on pyrope-spessartines this pyrope-almandine is substituted.

irregularities in this spectral region. Spectra of the nearly pure grossular (Fig. 5) almost replicate the previous measurements of other grossulars with low concentrations of impurity ions.[22,58]

The dielectric functions obtained from Kramers-Kronig analysis for samples 1, 2, 10, and 16 are classical in appearance and the resultant parameters (Table II) should be trustworthy. Sample 14 has a negative spike for the ϵ_2 dielectric function and the absorbance, which is attributed to an unresolved doublet at 449 cm^{-1}. The analysis is unreliable at lower wave numbers, and sample 14 is not used in comparisons of calculated with experimental *k*, although it illustrates the effect of high Ca content. For sample 1, also, ϵ_2 becomes slightly negative from the region between ~475 and 500 cm^{-1}, but the values appear credible.

Table II follows previous nomenclature[61] and band assignments.[22,23,54] The *P* mode is split in sample 16 into a Ca and an Fe peak, consistent with two-mode behavior[62] wherein peaks for the mixed crystal are seen at frequencies appropriate to the end members with intensities proportional to the amount of each end member component. Most peaks follow one mode behavior (Vegard's law) wherein the frequencies vary between those of the two end members.

The weak modes appearing in the gap between the Si-O stretching and O-Si-O bending regions are assigned to overtones. For sample 1, the *I* and *K* modes (441.1 + 376.4 cm^{-1} = 817.5 cm^{-1}) and the *F* and *O* modes (569.2 + 249.2 cm^{-1} = 818.5 cm^{-1}) together produce a very strong overtone observed at 813.0 cm^{-1}. The fundamentals implicated individually have high oscillator strengths, and this is responsible for the strength of the overtone. The peak at 814 cm^{-1} for sample 10 probably represents an overtone from a combination of the *H* and *M* modes (473.6 + 332.4 cm^{-1} = 806.0 cm^{-1}) and the *F* and *O* modes (567.9 + 243 cm^{-1} = 811 cm^{-1}). However, these modes are not as strong and so the overtone is not prominent. The *I* and *M* modes (450.7 + 332.4 cm^{-1} = 788.1 cm^{-1}) with the *E* and *Q* modes (644.5 + 136.9 cm^{-1} = 781.4 cm^{-1}) are implicated as the source of a weak overtone at 774 cm^{-1} in the same spectrum. The 432 cm^{-1} overtones in the spectra for 10 and 16 are more difficult to explain, but may represent incursions of an acoustic mode. Sample 16 shows no other overtones on a cursory analysis, although some overtones from strong modes such as the *I* and *K* (445.5 and 379.1 cm^{-1}), G_{Gr} and *M* (506.9 and 329.5 cm^{-1}), and *F* and *O* (568.3 and 240 cm^{-1}) may occur as features near the noise level. The spectrum of sample 14 is problematic enough that analysis of its overtones is futile. Sample 2 has no observable overtone combinations.

Table 2abc (accessible by EPAPS[60] or from the authors) gives complete IR reflectivity parameters from previous studies on other garnets relevant to this study.[22,23,58] For the synthetic garnets, the f_i and Γ_i values for the most intense peaks differ from the earlier report[24] due to an error in the computer program used in the classical dispersion analysis.

The FWHM for the mixed crystals is larger than those near the ends of the binary [cf. samples 40 to sample 3 in Table 2a (Ref. 60)]. The purest grossular (sample 2, Table II) has the narrowest peaks [see Table 2b] The differences are related to specific site substitutions, i.e., inclusion of Fe^{3+} appears to broaden peaks more than does Fe^{2+} (cf. sample B24 to EDN). For the pyrope-almandines, exchanging Ca for Fe^{2+} (at constant Mg) broadens the peaks [cf. sample 1 in Table II to sample 18 in Table 2a (Ref. 60)]. Substituting Ca for Mg (at constant Fe^{2+}) also broadens the peaks [cf. sample 10 in Table II to sample 40 in Table 2a (Ref. 60)]. Substitution of Ca in pyrope-almandine strongly affects the Si-O stretching modes, whereas the exchange of Mg-Fe mostly affects the low-frequency modes associated with cation translations.

VI. AVAILABLE EXPERIMENTAL VALUES OF THERMAL CONDUCTIVITY FOR GARNETS

To the best of our knowledge, Table III contains all published experimental values for *k* on natural garnets, excluding spessartines for reasons discussed below. Also included are synthetic yttrium garnets for which IR reflectivity data exist. Most of the thermal conductivity data were obtained 30 years ago and may be faulty, as suggested by inconsistent values of *k* among compositionally similar samples. Uncertainties in ascertaining sample compositions and suspected problems in the measured *k* values are summarized as follows.

Kanamori *et al.*[21] provide chemical compositions that are inconsistent with their reported values for the cell parameter and refractive index. These properties depend nearly linearly on compositions for most garnets.[19,46,63] Therefore, the compositions for their samples in Table III were calculated from their cell parameters and refractive indices, assuming that the samples are mixed crystals of pyrope, almandine, and grossular. Mn (spessartine) may be present, but minor amounts are unimportant to our analysis, as discussed below.

Horai[16] provides a locality and a density for his samples. His samples most likely came from the Francis Birch collection at Harvard, which has been discarded.[64] We requested chemical composition data from the author, but these are not available. Therefore, estimates of compositions for Horai's samples were made based on known garnet compositions from the source localities and by calculation from end member density values.[19]

The *k* value reported for sample H123 is close to *k* reported by Kanamori *et al.*[21] and Chai *et al.*[9] for similar garnets. The most recent study[9] involves a contact-free method and should be accurate, suggesting that the values of *k* near 3 W/m K for earlier studies of Ca-rich pyrope almandines represent the true values.

Diment and Pratt[65] provide densities and some description of their samples. Their two spessartines are porous, and the grossular sample has a low density, suggesting a large component of $4H^+$ substituting for Si^{4+}, and are thus dismissed from the comparison. The composition of their ''almandine'' is estimated from its density. However, its reported *k* is 30% lower than any other measurement, even for samples with similar chemistry (Table III). Because of this disparity, we conclude that Diment and Pratt's measurement of *k* for almandine-rich garnet is not reliable. Their other samples seem to be low by similar amounts compared to *k* of analagous samples.

Dreyer[66] provides only the mineral name ''almandine'' for his sample. Natural specimens of pure almandine are unknown.[19] We infer that the true composition is Al_{70} to Al_{90} by comparison of *k* values (Table III).

The compositions inferred for the pyrope-almandines are relatively reliable, probably within ~5 wt. %. The chemistry of these minerals tends to be uniform for a given locality. Pyrope-almandines usually include a few percent of Mn, but for our purposes, such low Mn content can be treated as if it were Fe^{2+}. This approximation is reasonable because spessartine and almandine spectra are nearly identical,[54] and their densities and sound speeds are similar.[67,68] Hence, the physical properties used to calculate *k* of almandine compare closely to those of spessartine, and their *k* values should be very close. Spessartine-rich garnets occur in nature, and *k* of such garnets is published[16,65] but the compositions cannot be reliably estimated. These samples are not considered further.

Grossular-andradites[16] have much less certain compositions, due to the common occurrence of impurities (e.g., H^+ and Ti^{4+}).[49,50] Sample H432, in particular, has a density about 0.27 g/cm^3 less than that of pure grossular, which implies considerable hydration, and therefore it cannot be accurately modeled using the available IR spectra of essentially dry samples.[22] Estimates of the compositions of Horai's other grossular-andradites in Table III primarily depend on compositions reported by other authors for garnets from the named localities. Sample H20, the only andradite, is probably the driest,[46,49,50] giving the most reliable composition.

Slack and Oliver[17] studied five natural garnets but list the *k* value only for grossular. Values for their other samples (Table III) were obtained from their log-log plots. Slack and Chrenko[69] provide chemical analyses of the same materials. Optical spectroscopy revealed noticeable levels of Fe^{3+}, but the andradite contents were not reported.[69] However, calibration curves[70] suggest that most of the Fe is divalent in the grossular. The peak heights in the optical spectra show that the hessonite has the same amount of Fe^{2+} as the grossular. From these considerations, we infer the compositions reported in Table III.

Slack and Oliver[17] also measured *k* of YAG, YIG, and YGG. Patel *et al.*[18] analyzed various samples in the solid-solution series YAG-YbAG, not including YAG, but presented results on *k* graphically only. Thermal conductivity results from Slack and Oliver[17] are generally higher than those reported by other authors for similar compositions (Table III). Their *k* values for YAG and both pyrope-almandines diverge from recent studies of similar materials,[9] and are thus suspect. Klein and Croft's[51] 30% higher measurement of 13 W/m K for YAG is clearly incorrect.

VII. CALCULATIONS AND DISCUSSION

A. Evaluation of the accuracy of the model

Thermal conductivity was calculated from Eqs. (10) and (11) using physical properties appropriate to the composition of each garnet with experimentally determined *k*. The FWHM were obtained from similar, but not exactly the same, garnets (Table III). The few problematic measurements discussed above were excluded from the comparison. Densities were obtained from linear interpolation.[19] Heat capacities depart from the assumed linearity, due the mixing effects in solid solutions, but this effect is small for pyrope-grossulars[63] and should be smaller still for the other series with lesser disparities in cation size. Sound speeds were linearly interpolated from existing data (Table III).

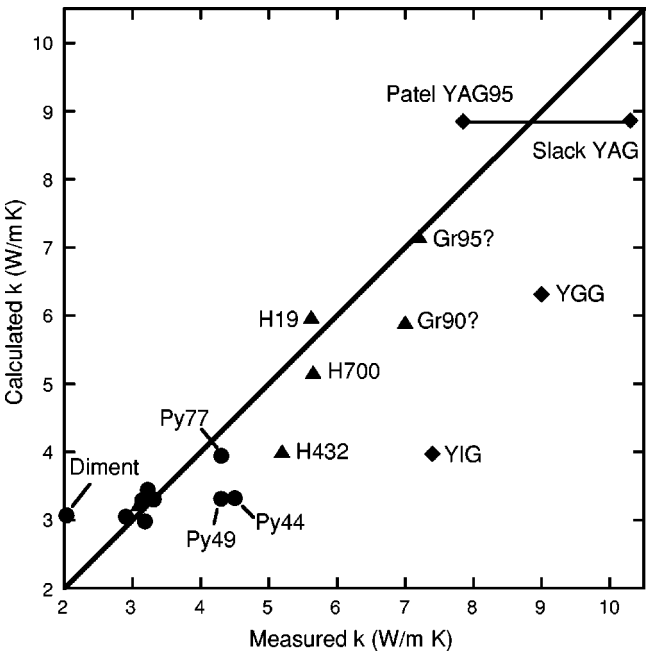

FIG. 6. Comparison of experimental and calculated thermal conductivity. Data from Table III. Circles: pyrope-almandine samples; triangles: grossular-andradite samples; diamonds: synthetic garnet samples. Samples with labels are discussed in the text. Py77, Py49, Py44, Gr95, and Gr90 samples from Slack and Oliver (Ref. 17).

The results (Table III, Fig. 6) are in excellent agreement with experiment, considering the experimental uncertainties in both composition and *k*. Uncertainties in the input parameters are small in comparison. Figure 6 shows an excellent match of calculated *k* with measurements that have been confirmed by multiple studies on similar material, and recapitulates the problems inferred from comparing the various experimental determinations with each other.

Measurements of *k* for pyrope-almandines from several studies cluster near 3.3 W/m K, and these values are returned by Eq. (11), within a nominal experimental uncertainty of ~5%. The calculation for pyrope-spessartine is in good agreement with the measurement of Slack and Oliver[17] given the need to approximate the input parameters for the spessartine component, and our estimation of *k* from a graph. However, their pyrope-almandine samples have thermal conductivities that are ~25% higher than the calculation. This difference is almost certainly due to experimental errors as similar garnets have lower *k*.[9] The thermal conductivity measurement of Diment and Pratt[65] is substantially lower than any of the other measured results for pyrope-almandines (Table III), and can be discounted. The disparities of 25–33 % seen between these measurements and the calculations (Table III) is the same size as that found in interlaboratory

TABLE IV. Physical data and calculated thermal conductivity of spectral samples. Peak widths from certain samples on this table were used to construct model values of thermal conductivity in Table III (they are identified there), but the physical data in this table is adjusted to the composition of these samples themselves. Table headings are similar to those in Table III. *M*: molecular weight. YIG and YGG are omitted since all data would be identical to Table III.

Sample	Composition	Avg. FWHM [a] cm^{-1}	ρ [b] g/cm^3	M g/mol	C_V [c] J/mol K	u_P km/s	u_S km/s	k W/m K
3	$Py_{95}Al_4Gr_1$	9.4	3.61	407.39	326.00	9.10 [e]	5.08 [e]	5.59
18	$Py_{72}Al_{28}$ [m]	12.9	3.79	429.62	330.84	8.92 [d]	5.00 [d]	3.97
1	$Py_{71}Al_{18}Sp_1Gr_{10}$ [m]	17.0	3.74	429.62	331.22	8.90 [l]	5.00 [l]	2.97 [i]
40	$Py_{58}Al_{39}Sp_1Gr_2$ [m]	14.6	3.95	441.90	332.87	8.83 [k]	4.96 [k]	3.45
14	$Py_{52}Al_{21}Gr_{27}$	17.2	3.74	435.78	330.77	8.95 [f]	5.01 [f]	2.91 [i]
10	$Py_{47}Al_{40}Gr_{13}$	16.5	3.88	447.13	333.46	8.83 [d]	4.99 [d]	3.04 [i]
16	$Py_{41}Al_{45}Sp_1Gr_{13}$ [m]	15.0	3.92	452.78	334.50	8.77 [l]	4.93 [l]	3.29 [i]
33	$Py_{44}Al_{50}Gr_6$	15.1	3.95	453.28	334.90	8.77 [l]	4.93 [l]	3.30
11	$Py_{18}Al_{82}$	11.8	4.19	480.72	340.18	8.59 [l]	4.82 [l]	4.10
41	Al_{100}	9.6	4.32	497.75	343.29	8.43 [d]	4.73 [d]	4.86
B43	$Gr_{1.5}An_{98.5}$	9.1	3.86	507.31	351.56	8.50 [g]	4.84 [g]	4.77
B44	$Gr_{29}An_{71}$	13.5	3.78	491.44	345.60	8.47 [l]	4.96 [l]	3.26
B35	$Gr_{47}An_{51}Sp_2$	15.3	3.74	479.90	341.53	8.72 [d]	5.11 [d]	3.07
M	$Gr_{64}An_{36}$	15.9	3.69	471.20	338.02	8.89 [d]	5.21 [d]	3.05
B28	$Gr_{80}An_{20}$	11.5	3.65	462.00	334.55	9.04 [l]	5.30 [l]	4.34
B51	$Gr_{88}An_9Py_3$ [m]	10.1	3.64	454.23	331.58	9.16 [d]	5.36 [d]	5.21
EDN	$Gr_{91}An_4Al_5$	8.9	3.64	455.13	331.79	9.21 [d]	5.42 [d]	5.79
B24	$Gr_{95}An_5$	8.7	3.61	453.35	331.30	9.26 [d]	5.46 [d]	6.08
B12	$Gr_{99}An_1$	7.4	3.60	451.04	330.44	9.33 [h]	5.50 [h]	7.24
2	$Gr_{99.5}Al_{0.5}$	6.3	3.60	450.69	330.29	9.33 [h]	5.50 [h]	8.43
YAG	$Y_{94.5}Sm_{5.5}AG$	5.4	4.64	603.81	371.20	8.52 [j]	4.97 [j]	8.88

[a] See Tables II and III.

[b] Densities calculated as linear combinations of the end member density [i.e., assumes ideal mixing (Refs. 19, 63)]. Endmember densities for natural garnets taken from Deer *et al.*[19] Density for sample YAG calculated from formula weight and cell volume.

[c] Interpolated from endmember values: pyrope (Ref. 54), almandine, grossular, and andradite (Ref. 80).

[d] Interpolation/extrapolation from existing data.

[e] Data for pure pyrope (Ref. 84).

[f] Value is speculative for such high grossular content.

[g] Data for pure andradite (Ref. 85).

[h] Data for pure grossular (Ref. 72).

[i] On account of the high grossular content of these samples, these values are plotted separately in Fig. 6.

[j] Yogurtçu *et al.* (Ref. 81).

[k] For garnet with composition $Py_{62}Al_{36}Gr_2$ (Ref. 73).

[l] For garnet with similar composition (Ref. 67).

[m] One of the minor components represents the sum of similar components, since their effect on *k* at such low concentrations is practically identical. For Sample 1, Gr includes Gr+An+Uv. For B51, Py includes Py+Al+Sp. For samples 16 and 40, Al includes Al and Sp. See the sources (Refs. 22, 23) for precise compositions.

comparisons.[2] Based on known difficulties in accurately measuring *k*, and on the good agreement of the calculation with the five points in the cluster of pyrope-almandines and with the sole pyrope-spessartine, Eqs. (10) and (11) accurately represent this type of garnet.

The grossular-andradites provide a less stringent test due to fewer measurements, and to uncertain compositions. The calculation for the sample with high andradite content, which should be relatively dry, matches experiment (Fig. 6). The average of the calculated values for two grossular-rich samples of Horai[16] equals the experimental determination. The spread occurs because the water and Fe content affect the density in opposite directions and the samples probably have compositions diiffering from our estimates. Agreement is unsatisfactory for Horai's sample H432 because this could contain $\sim$50% hydrogarnet or consist of multiple phases, based on its density. Its input parameters (Table III) are rough estimates. Similarly, the calculation matches experimental *k* for the purer of the two grossulars from Slack and Oliver.[17] Their ''hessonite'' sample has double the Fe content, with both ferric and ferrous species, but its experimental *k* is no different than the nearly pure grossular (Table III).

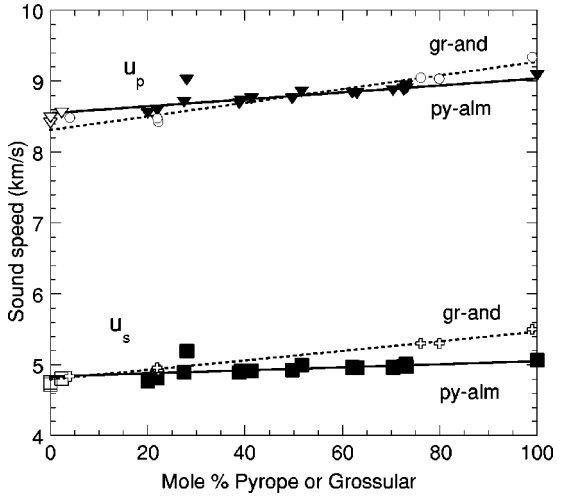

FIG. 7. Compiled sound velocity data for each of the pyrope almandine and the grossular-andradite series (Refs. 67 and 72–74). Lines indicate linear fits to the data. Open squares and triangles represent almandine-pyrope samples rich in Mn.

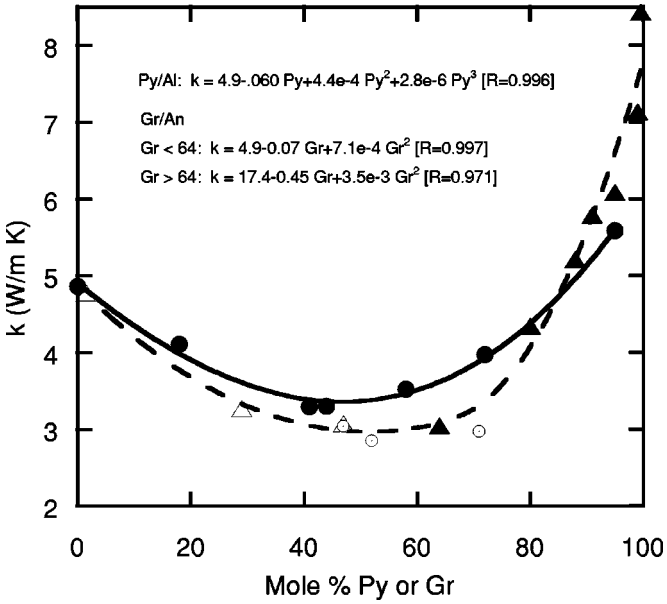

FIG. 8. Dependence of calculated thermal conductivity on composition for the pyrope-almandine and grossular-andradite systems. Filled circles and solid line: the pyrope-almandine samples fit with a cubic polynomial; open diamonds and dashed line: the high-andradite trend fit with a quadratic polynomial; filed triangles and dashed line: the high-grossular trend fit with a quadratic polynomial. Open circles: pyrope-almandine samples with high concentrations of grossular or other garnets and wider peak widths, which lower their model values for thermal conductivity relative to purer pyrope-almandines.

This hessonite has k more than 1.5 W/m K higher than k of similarly impure grossulars (Fig. 6), suggesting that this value is too high.

For the yttrium garnets, few samples were measured and disagreements exist among the data. The experimental values of YAG provide a weak test. The thermal conductivity calculated using FWHM from YAG doped with 5.5% Sm lies close to the average of the experimental determinations (Fig. 6, Table III) for YAG (Ref. 17) and for YAG doped with 5% Yb.[18] Patel *et al.*[18] obtained nearly the same k for 15% Yb as for 5%, suggesting that their k value for 5% dopant is slightly low (see the next section). At such low impurity levels, substitution of different lathanide ions is unlikely to matter, suggesting that the calculation (Table III) probably provides the correct k at 5% dopant. The experimental value for pure YAG by Slack and Oliver[17] should be within 5% of the true value. This inference is based on the decrease of FWHM of grossular as impurity level decreases, and on our underestimate of k for YAG based on $\langle\Gamma\rangle$ of a Sm-doped sample (Table III).

Our model agrees poorly with the determinations of Slack and Oliver[17] of k for YGG and YIG (Fig. 6). Neither experimental result has been corroborated. The YGG value is 30% high: a discrepancy between experiments of this size is common.[2] We believe our value for YGG represents the true k, within 5 to 6%, because the IR spectra were high quality and all peaks were observed (Table 2c),[60] although the widths of two could not be accurately determined. In contrast, the peak widths obtained for YIG are high compared to YAG and YGG and several of the weak peaks are uncertain.[24] Although the large FWHM explains why k of YIG is lower than that of YGG, in agreement with the experimental data, $\langle\Gamma\rangle$ seems overly large, and so our model value is probably low for YIG. Slack and Oliver's value for YIG is too high, but is probably not 45% too large, as suggested by the calculation.

B. Relationship of thermal conductivity to physical properties

To understand the effect of the various physical parameters in Eqs. (10) and (11) on k, the calculations were repeated based on the known chemical compositions of the samples with IR spectra (Table IV). Density, molar weight, and C_V, were obtained from linear interpolation based on their compositions. The sound speeds of pyrope-almandines depend linearly on composition; the grossular-andradites also form a linear trend (Fig. 7). From this, we calculated the sound speeds of all samples based on the proportions of the end members (Table IV).

Both the pyrope-almandine and the grossular-andradite series have a k that is higher for the end members than for the intermediate solid solutions (Fig. 8). Our calculation for the grossular-andradite binary mimics the experimentally determined curve for the system YAG-YbAG, which has a minimum at 60% YAG and a steep slope associated with the end member (YAG) that has the higher thermal conductivity, whereas the trend towards the low-conductivity end member is shallow.[18] Experimental determinations for k in the systems $NaAlSi_3O_8$-$CaAl_2Si_2O_8$ and Mg_2SiO_4-Fe_2SiO_4 behave analogously.[16]

Thermal conductivity over the pyrope-almandine series is described by a cubic fit (Fig. 8). Four of the pyrope-almandine samples in Table IV were excluded from the curve fitting due to their high Ca^{2+} contents. Because the Ca^{2+} ion is noticeably larger than the Mg^{2+}, Fe^{2+}, or Mn^{2+} ions, adding Ca^{2+} distorts the crystal lattice,[47,48] widens the peaks

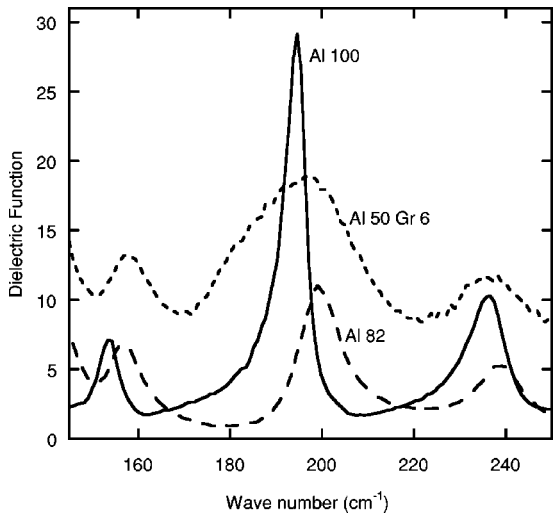

FIG. 9. Calculated values of ϵ_2 for samples 41 (Al_{100}), 11 ($Al_{82}Py_{18}$), and 33 ($Al_{50}Gr_6Py_{44}$), showing the widening of cation-translation peaks with increasing disorder on the *X* lattice site. Most modes behave similarly.

(Table II, Fig. 9), and lowers the thermal conductivity (Fig. 8). From the Py-Al trend, Dreyer's[66] ''almandine'' sample contains about 30% pyrope.

The grossular-andradite binary could not be adequately fit to any polynomial. Instead, the data were modeled by two quadratic fits for the high-Al and high-Fe^{3+} ends of the curve (Fig. 8). This complicated fit is needed to describe the asymmetry of the Gr-An series, particularly the steep rise at high Gr content (Fig. 8). Such a steep rise probably does not occur at high Py content for the Py-Al binary because pyrope-rich samples have two pairs of IR peaks that are degenerate,[23] providing a large FWHM, which limits the rise. The steep trend observed for doped YAG samples occurs because YAG, similar to grossular, has narrow and well-resolved IR peaks.

The model predicts $k = 8–8.5$ W/m K for grossular, 6 W/m K for pyrope, and 5 W/m K for almandine and andradite (Table IV). The thermal conductivity of spessartine and uvarovite should also be about 5 W/m K. From Fig. 8 and the experimental data (Table III), garnets with a high degree of solid solution (i.e., most natural garnets) will have *k* between 3 and 3.5 W/m K.

The nonlinear dependence of *k* (Fig. 8) must be due to changes in the FWHM because all the other physical properties in Eqs. (10) and (11) depend nearly linearly on composition (Fig. 7). The average FWHM has a minimum near the middle of the two binaries examined here (Fig. 10). The asymmetry of the thermal conductivity curves (Fig. 8) is also repeated in the FWHM (Table IV, Fig. 10). The precise nature of the compositional dependence of FWHM is complicated by factors such as accidental degeneracy. Chemistry appears also to be a factor as the Fe^{3+} end members for both the Ca and Y garnets have broader peaks. Two-mode behavior[62] pertains because the existence of local modes provides additional opportunities for phonon-scattering; hence, lifetimes are shorter and peaks are broader overall. One-mode behavior can also provide peak broadening.[71] The underlying reason for the mimima in the average FWHM is disorder on the sites. The existence of the minima near the middle of both series and the similar values for the average FWHM near the minimum suggests that grossular-andradite series is disordered by the same amount as the pyrope-almandine series. Thus, the birefringence seen for these samples, which is common in such garnets, is not compatible with ordering on the various sites.

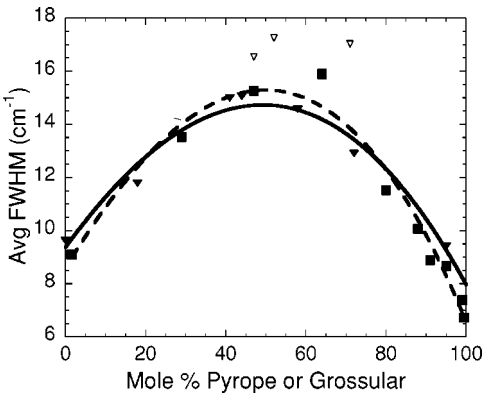

FIG. 10. Compositional dependence of the FWHM (Tables II, III, and IV). Triangles with solid line: pyrope-almandines; open triangles: pyrope-almandines with high Ca which are not included in the curve fit. Squares and broken line: grossular-andradites. The lines are cubic fits.

The importance of the FWHM to the thermal conductivity is emphasized in Fig. 11, which shows that the measured *k* correlates linearly with the average FWHM from garnets with similar composition. This correlation has scatter because the sound speeds and other relevant parameters in Eq. (11) are not accounted for. The correlation (Fig. 11) emphasizes the wide variation in FWHM that is possible for one given structure, and confirms that phonon-scattering lifetimes are represented by FWHM in IR spectra.

VIII. CONCLUSIONS

The results affirm the validity of utilizing phonon lifetimes implicit in the damped harmonic oscillator model in

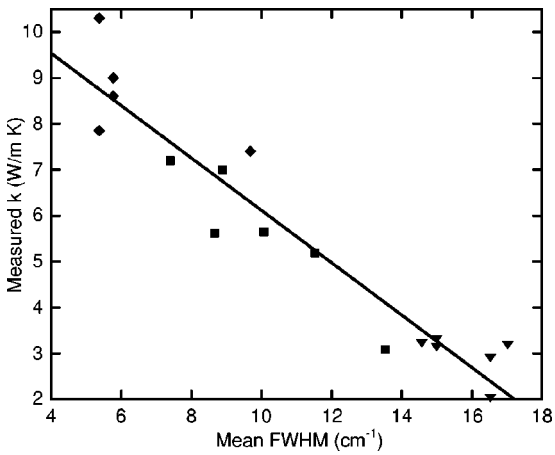

FIG. 11. Relationship of measured thermal conductivity to IR peak widths obtained from similar samples (Table III). Triangles: pyrope-almandines; squares: grossular-andradites; diamonds: synthetic garnets. The solid line is a linear fit to the data; $R = 0.95$.

Debye's model of thermal conductivity, which treats phonon scattering as analogous to the kinetic theory of gases. The model replicates k at ambient conditions when the experimental data are confirmed through multiple studies and when the chemistry of the sample is known. The model provides a compositional dependence similar to that observed experimentally.

For the various garnets examined here, the weighted average [Eq. (10)] represents the average sound speeds relevant to calculating the thermal conductivity. Garnets have 240 total vibrational modes. For olivines and spinels with 84 and 42 total modes, a simple average of the sound speeds, was found to reproduce experimental values of k.[5] It is not clear whether the type of average used to compute u from the sound speed depends on the structure, or only on the number of modes. Examination of substances with other structures and with differing numbers of total vibrational modes is needed.

For the garnets, as previously shown for olivines and spinels,[5] the model is accurate to 5% when the input parameters are known. This accuracy rivals that of modern experimental methods.[9,12] It allows evaluation of the accuracy of the earlier datasets, resolution of discrepancies, and prediction of k for intermediates and end-member compositions. However, being a phenomenological theory, application to other structures requires calibration against reliable experimental data, to ascertain the relationship between u and the sound speeds.

ACKNOWLEDGMENTS

This research was supported by NSF, Grant No. EAR-9712311. We thank R. M. Hazen and J. R. Smyth for providing samples; K. M. Campbell, T.J. Fagan, and R. B. Schaal for help with spectal data acquisition and microprobe analysis; and J. D. Pasteris for helpful input. This paper represents the senior thesis of P.A.G.

[1] D. A. Yuen, A. P. Vincent, S. Y. Bergeron, F. Dubuffet, A. A. Ten, V. C. Steinbach, and L. Starin, in *Problems in Geophysics for the New Millenium*, edited by E. Boschi, G. Ekstrom, and A. Morelli (Editrice Compositori, Bologna, Italy, 2000), pp. 405–465.
[2] R. G. Ross, P. Andersson, B. Sundqvist, and G. Backstrom, Rep. Prog. Phys. **47**, 1347 (1984).
[3] Y. H. Lee, R. Biswas, C. M. Soukoulis, C. Z. Wang, C. T. Chan, and K. M. Ho, Phys. Rev. B **43**, 6573 (1991).
[4] A. M. Hofmeister, Science **283**, 1699 (1999).
[5] A. M. Hofmeister, Am. Mineral. **86**, 1188 (2001).
[6] P. Debye, *Vortrage uber die kinetische Theorie der Materie und der Electrizitat* (B. G. Teuber, Berlin, 1914).
[7] R. Peierls, Ann. Phys. (Leipzig) **3**, 1055 (1929).
[8] P. G. Klemens, Solid State Phys. **7**, 1 (1958).
[9] M. Chai, J. M. Brown, and L. Slutsky, Phys. Chem. Miner. **23**, 470 (1996).
[10] G. Slack, Solid State Phys. **34**, 1 (1979).
[11] A. Einstein, Ann. Phys. (Leipzig) **35**, 679 (1911).
[12] D. Cahill, S. K. Watson, and R. O. Pohl, Phys. Rev. B **46**, 6131 (1992).
[13] R. T. Beyer and S. V. Letcher, in *Physical Ultrasonics* (Academic Press, New York, 1969), p. 257.
[14] G. Burns, *Solid State Physics* (Academic Press, San Diego, 1990).
[15] G. Slack, Phys. Rev. **126**, 427 (1962).
[16] K. Horai, J. Geophys. Res. **76**, 1278 (1971).
[17] G. Slack and D. W. Oliver, Phys. Rev. B **4**, 592 (1971).
[18] F. D. Patel, E. C. Honea, J. Speth, S. A. Payne, R. Hutcheson, and R. Equall, IEEE J. Quantum Electron. **37**, 135 (2001).
[19] W. A. Deer, R. A. Howie, and J. Zussman, *Introduction to the Rock-Forming Minerals* (Wiley, New York, 1992).
[20] D. J. Weidner and Y. Wang, *Earth's Deep Interior: Mineral Physics and Tomography from the Atomic to the Global Scale*, Vol. 117 of *Geophysical Monograph* (American Geophysical Union, Washington, D.C., 2000), pp. 215–235.
[21] H. Kanamori, N. Fujii, and H. Mizutani, J. Geophys. Res. **73**, 595 (1968).
[22] B. P. McAloon and A. M. Hofmeister, Am. Mineral. **80**, 1145 (1995).
[23] A. M. Hofmeister, T. J. Fagan, K. M. Campbell, and R. B. Schall, Am. Mineral. **81**, 418 (1996).
[24] A. Hofmeister and K. R. Campbell, J. Appl. Phys. **72**, 638 (1992).
[25] A. Einstein, Ann. Phys. (Leipzig) **22**, 180 (1907).
[26] F. Reif, *Fundamentals of Statistical and Thermal Physics* (McGraw-Hill, New York, 1965).
[27] W. G. Spitzer, R. C. Miller, D. A. Kleinman, and L. W. Howarth, Phys. Rev. **126**, 1710 (1962).
[28] G. Andermann, A. Caron, and D. A. Dows, J. Opt. Soc. Am. **55**, 1210 (1965).
[29] F. Wooten, *Optical Properties of Solids* (Academic Press, San Diego, 1972).
[30] S. S. Mitra, in *Optical Properties of Solids*, edited by S. Nudelman and S. S. Mitra (Plenum Press, New York, 1969), pp. 333–452.
[31] R. F. Gallup and L. B. Coleman, Phys. Chem. Miner. **17**, 271 (1990).
[32] A. Kachare, G. Andermann, and L. R. Brantley, J. Phys. Chem. Solids **33**, 467 (1971).
[33] A. M. Hofmeister and H. K. Mao, Am. Mineral. **86**, 622 (2001).
[34] C. I. Merzbacher and W. B. White, Am. Mineral. **73**, 1089 (1988).
[35] J. A. Bardwell and M. J. Dignam, J. Chem. Phys. **83**, 5468 (1985).
[36] F. Stern, Solid State Phys. **15**, 300 (1963).
[37] W. F. Oliver, C. A. Herbst, S. M. Lindsay, and G. H. Wolf, Rev. Sci. Instrum. **63**, 1884 (1992).
[38] N. W. Ashcroft and N. D. Mermin, *Solid State Physics* (Holt, Rinehart and Winston, New York, 1976).
[39] M. Born and K. Huang, *Dynamical Theory of Crystal Lattices* (Oxford University Press, New York, 1954).
[40] S. W. Kieffer, Rev. Mineral. **14**, 65 (1985).
[41] P. Debye, Ann. Phys. (Leipzig) **39**, 789 (1912).
[42] S. W. Kieffer, Rev. Geophys. Space Phys. **17**, 20 (1979).
[43] M. Born and T. von Karman, Phys. Z. **13**, 297 (1912).

[44] H. Bilz and W. Kress, in *Solid-State Sciences*, edited by M. Cardona, P. Fulde, and H.-J. Quessier (Springer Verlag, Berlin, 1979), Vol. 10, pp. 1–231.
[45] K. R. Symon, *Mechanics* (Addison-Wesley, Reading, MA, 1971).
[46] E. P. Meagher, Rev. Mineral. **5**, 25 (1980).
[47] M. Merli, A. Callegari, E. Cannillo, F. Caucia, M. Leona, R. Oberti, and L. Ungaretti, Eur. J. Mineral. **7**, 1239 (1995).
[48] L. Ungaretti, M. Leona, M. Merli, and R. Oberti, Eur. J. Mineral. **7**, 1299 (1995).
[49] G. R. Rossman and R. D. Aines, Am. Mineral. **76**, 1153 (1991).
[50] G. Amthauer and G. R. Rossman, Am. Mineral. **83**, 835 (1998).
[51] P. H. Klein and W. J. Croft, J. Appl. Phys. **38**, 1603 (1967).
[52] Q. Bi, J. M. Brown, and Y. Sato-Sorensen, J. Appl. Phys. **68**, 5357 (1990).
[53] R. K. Moore, W. B. White, and T. V. Long, Am. Mineral. **56**, 54 (1971).
[54] A. M. Hofmeister and A. Chopelas, Phys. Chem. Miner. **17**, 503 (1991).
[55] D. T. Griffen, *Silicate Crystal Chemistry* (Oxford University Press, New York, 1992).
[56] A. B. Chase and R. A. Lefever, Am. Mineral. **45**, 1126 (1960).
[57] A. M. Hofmeister *et al.*, Am. Mineral. **83**, 1293 (1998).
[58] B. P. McAloon and A. M. Hofmeister, Am. Mineral. **78**, 957 (1993).
[59] K. Kingma and J. Downs, Am. Mineral. **74**, 1307 (1989).
[60] See EPAPS Document No. E-PRBMDO-65-163213 for additional tables. This document may be retrieved via the EPAPS homepage (http://www.aip.org/pubservs/epaps.html) or from ftp.aip.org in the directory /epaps/. See the EPAPS homepage for more information.
[61] P. Tarte, Mem. Acad. R. Belg. **35**, 1 (1965).
[62] I. F. Chang and S. S. Mitra, Phys. Rev. **172**, 924 (1968).
[63] H. T. Haselton, Jr. and E. F. Westrum, Jr., Geochim. Cosmochim. Acta **44**, 701 (1980).
[64] Carl Francis (private communication).
[65] W. H. Diment and H. R. Pratt, *Thermal Conductivity of Some Rock-Forming Minerals* (Open-File Report 88-690, USGS, Washington, D. C., 1988).
[66] W. Dreyer, *Materialverhalten Anisotroper Festkorper: Thermische und Electrische Eigenschaften* (Springer, Vienna, 1974).
[67] V. Babuška, J. Fiala, M. Kumazawa, I. Ohno, and Y. Sumino, Phys. Earth Planet. Inter. **16**, 157 (1978).
[68] J. D. Bass, in *Mineral Physics and Crystallography: A Handbook of Physical Constants*, edited by T. J. Ahrens (American Geophysical Union, Washington, DC, 1995), pp. 45–63.
[69] G. Slack and R. M. Chrenko, J. Opt. Soc. Am. **61**, 1325 (1971).
[70] W. B. White and R. Moore, Am. Mineral. **57**, 1692 (1972).
[71] P. Burns, F. C. Hawthorne, A. M. Hofmeister, and S. L. Moret, Phys. Chem. Miner. **23**, 141 (1996).
[72] J. D. Bass, J. Geophys. Res. **94**, 7621 (1989).
[73] S. L. Webb, Phys. Chem. Miner. **16**, 684 (1989).
[74] M. Chai, J. M. Brown, and L. Slutsky, Geophys. Res. Lett. **24**, 523 (1997).
[75] F. R. Boyd, Year Book-Carnegie Inst. Washington **73**, 285 (1974).
[76] F. A. Capoiscio and J. R. Smyth, Contrib. Mineral. Petrol. **105**, 550 (1990).
[77] S. B. Levin, Geol. Soc. Am. Bull. **61**, 519 (1950).
[78] A. Pabst, Am. Mineral. **21**, 1 (1936).
[79] W. Agar and P. Krieger, Am. J. Sci. **5**, 68 (1932).
[80] R. A. Robie and B. S. Hemingway, *Thermodynamic Properties of Minerals and Related Substances at 298.15K and 1 bar (10^5 Pascals) Pressure and High Temperature* (Bulletin 2131, USGS, Denver, 1995).
[81] Y. K. Yogurtcu, A. J. Miller, and G. A. Saunders, J. Phys. C **13**, 6585 (1980).
[82] D. E. Eastman, J. Appl. Phys. **37**, 2312 (1966).
[83] E. V. Zharikov, V. F. Kitaeva, and V. Y. Fedorovich, Fiz. Tverd. Tela (Leningrad) **31**, 217 (1989).
[84] B. O'Neill, J. D. Bass, J. R. Smyth, and M. T. Vaughan, Phys. Chem. Miner. **17**, 617 (1991).
[85] J. D. Bass, J. Geophys. Res. **91**, 7505 (1986).